Contact of Crack Surfaces during Fatigue: Part 2. Simulations

HUSEYIN SEHITOGLU and ANA MARÍA GARCÍA

A detailed model of the role of asperities in crack closure has been initiated in Part 1 of this article. Crack opening stress is defined as the far-field stress required to overcome the asperity-induced contact stresses along the crack. In this Part 2, the magnitude of crack opening stress is established as a function of roughness (σ_0); asperity density (N); maximum stress level (S_{max}/S_y); shakedown pressure (p_0^s/k), which reflects the effect of tangential tractions or friction; R ratio; and crack length. Normalizations permit application to a wide range of materials. The results, for selected levels of asperity density, are consolidated upon comparing the crack opening displacement (COD) with the roughness (σ_0) over four orders of magnitude. Specifically, a nonlinear relationship between COD/σ_0 and crack opening stress was established that can be readily used to determine crack opening stress over a broad range of conditions. The model has been utilized to predict crack opening stress levels for several materials, including 0.8 pct C steels, 9Cr-1Mo steels, Ti-4Al, Ti-46Al (γ-aluminide), and Al 2124 alloys. Experimental measurements of crack roughness and asperity density were conducted on titanium aluminide specimens using confocal microscopy, and crack closure predictions were made with the model. The predictions demonstrated very good agreement with the experimentally measured closure levels.

I. INTRODUCTION

THE modification of the stress intensity factor based on crack closure has been universally applied to explain the experimental observations of fatigue crack growth behavior under various mechanical loading conditions and in various metallic alloys. For an overview of the topic, the reader is referred to the textbook by Suresh[1] and the overview by Sehitoglu *et al.*[2] However, to develop a better understanding of the intrinsic mechanisms of crack growth in various materials due to mechanical and microstructural factors, it is particularly important to determine the individual influences of crack closure due to plasticity, roughness, and oxide effects. Then, the effect of each of these mechanisms can be isolated to develop more advanced models for crack advance. Since a quantitative description of crack roughness effects has not been previously derived, the present work has undertaken this task.

In many materials, when the crack advance is influenced by crystallographic slip or when the crack encounters microstructural barriers, the crack paths are nonflat and the crack can deviate from the normal mode I growth plane. The nonflatness of crack surfaces has been known to enhance the resistance of a material to fatigue crack growth. This resistance can develop in cases when the crack surfaces are viewed as nominally flat at the macrolevel, but there could be many periodic deviations from a smooth crack surface in the forms of asperities at the microlevel. These asperities could interlock at very low loads, or slide and crush in the presence of sufficient loading, resulting in an alteration of the crack surface profile as the crack advances. Combining the interaction of many asperities results in stresses in the crack wake which, in turn, have to be overcome before the crack can move forward. Therefore, the calculation of the driving force on the crack in the presence of complex crack surface interaction represents one of the present challenges to fatigue crack propagation analyses. As will be discussed subsequently, almost all classes of materials, with suitable heat treatment or processing, can be made to exhibit nonflat crack surfaces which will undergo contact due to the presence of asperities. Due to the significance of the problem, many experimental studies from the materials science community have documented the role of crack roughness effects in the literature. On the other hand, the modeling of the crack surface interference *via* asperity sliding and crack closure has received much less consideration.

The few models forwarded to capture the crack deflection on crack growth rates can be divided into two categories: those that consider isolated cases of periodic tilting and those that consider discrete asperity locking. In the case of deflection of a tensile crack from the nominal mode I plane, mixed-mode crack tip conditions develop, and these can be handled in the context of fracture mechanics (assuming crack closure does not occur). Under cyclic loading conditions, however, the change in the crack growth path will result in enhanced interference of crack surfaces, and a general model has not emerged that addresses this condition. A few attempts to analyze a single asperity behind the crack tip have been reported, but they are not sufficient to accurately describe the interference over the entire crack face.

In Part 1 of this article,[3] the authors used ''contact mechanics'' concepts to analyze the stresses behind the crack tip, and these concepts were used to determine the reduction in the crack tip driving force. In Part 2 of the article, we consider various far-field loading conditions (mostly nominally mode I conditions) and the role of shear tractions, and we compare the predictions to experimental findings to develop as much insight into the problem as possible. We do not consider the closure effects associated with oxides and other debris in the crack wake, or the plasticity-induced closure that has been rather well studied. We also note that

HUSEYIN SEHITOGLU, Professor and Associate Head, and ANA MARÍA GARCÍA, Research Assistant, are with the Department of Mechanical and Industrial Engineering, University of Illinois, Urbana, IL 61801.

Manuscript submitted March 5, 1997.

the roughness of crack surfaces can be rather nonuniform in the thickness direction, but, as a first approximation, we assumed that the entire crack front undergoes the same deflections and deviations along the thickness direction (*i.e.*, plane strain conditions). Furthermore, the analysis conducted in this work does not consider microstructural (crystallographic) slip and, hence, treats the contacting asperities with continuum plasticity.

Early Experimental Observations

Following the initial observations of highly deflected crack surfaces in underaged alloys, researchers began to quantify the macroscopic phenomenon of closure and to directly link it to the crack growth-rate behavior and the threshold stress intensity. A schematic of the nonlinear crack paths and the mechanisms is in Figure 1. Many of these experimental works were concerned with crack growth behavior in the near-threshold regime for materials which presented similar stress-strain properties yet differed considerably in microstructure. It is well established that Al alloys with underaged conditions produce a crystallographic crack which is highly nonflat, while the same material in the overaged heat-treatment condition leads to a flat crack.[4,5,6] The reason for the highly deflected crack profile in the underaged case is that the underaged precipitates that are coherent are sheared by dislocations, promoting planar slip (Figure 1(a)). On the other hand, the overaged precipitates that are incoherent are bypassed by dislocations; the resulting deformation mode is one of duplex or multiple slip, and the crack exhibits a flat profile. Similar results hold for precipitation-hardened nickel-based superalloys.[7] Also, when the plastic zone of the crack is larger than the small microstructural dimension such as the grain size or precipitation spacing, the crack process zone undergoes multiple slip and the crack growth profile is planar. On the other hand, when the crack is driven at low loads, the plastic zone size could be smaller than the limiting microstructural dimension, resulting in localized variations from a planar path. In Figure 1(b), the nonlinear crack path due to a lamellar structure such as that observed in pearlitic steels is shown.[8] Within an austenite grain several pearlite colonies exist, each with different lammellae orientation. The crack path often follows the interfaces of the lamellae with periodic fracture perpendicular to the lamellae. Other examples of the nonlinear crack paths are encountered in duplex microstructures, ferritic-pearlitic microstructures, and ferritic-martensitic microstructures (Figure 1(c)).[9] Finally, the crack path could be nonlinear, since the orientation of the most favorable slip direction varies due to different grain orientations along the crack path. This is shown in Figure 1(d), where the angles ϕ and Θ denote grain orientation and angle between the two slip systems, respectively.[2,10]

Experimental observations of roughness effects and closure measurements have been conducted on three classes of alloys, namely, the Al alloys, Ti alloys, and steels. Carter *et al.*[5] demonstrated that the threshold stress intensity range differed depending on the grain size and the underaged *vs* overaged condition of the Al 7475 alloy. The threshold stress intensity increased as the grain size increased, in the range of 18 to 80 μm. Blankenship and Starke[6] demonstrated that the Al-Cu-Li alloys exhibit a nonflat crack profile in the T3 (underaged) condition and nearly flat profiles for the T8 (overaged) condition. In an early work, Ritchie *et al.*[4] considered the underaged and overaged microstructures of Al alloy 2124. They measured closure levels of K_{clos}/K_{max} = 0.65 for the underaged microstructure.

Ti-6Al-4V alloys result in a microstructure with an α and retained β or an acicular α microstructure. Walker and Beevers[11] noted the irregular crack paths in this class of alloys nearly 20 years ago. The acicular structure leads to a more nonlinear crack path. Larsen[12] worked on two compositions of a Ti-Al alloy. Increasing the Al content from 4 to 8 pct resulted in a planar-slip deformation in these alloys. Larsen defined a ''roughness'' parameter by dividing the profile crack length by the crack length projected normal to the load axis. Thus, fracture surface roughness increased with this parameter. He found that the roughest microstructure this parameter was 1.452, and the opening level was highest (K_{open}/K_{max} = 0.80). It was clear from their study that modified ΔK studies based on deflected crack length are not sufficient to capture the crack growth behavior, and inclusion of crack closure was necessary. Allison *et al.*[13] studied the role of crack roughness on crack growth behavior of two microstructures of Ti-6242S alloys. The coarse microstructure (the β phase, with grain size $\approx$100 to 200 μm) presented considerably high opening levels (K_{open}/K_{max} = 0.6). Ogawa and Tokaji[14] made similar observations when they studied three microstructures of Ti-6Al-4V. Their maximum closure levels exceeded 0.6 of the maximum stress. They measured roughness in a similar manner to Larsen, by defining an area ratio of the three-dimensional image of a fracture surface to the projected area. The opening level for the microstructure with the highest area ratio of 2.0 was found to be K_{open}/K_{max} = 0.6.

Gray *et al.*[8] analyzed the effects of grain, colony size, and pearlite spacing effect in pearlitic steels as they influence fatigue crack growth. They showed that these microstructural features had an effect on near-threshold crack growth in as much as they increased the level of roughness. Fracture surface topography was quantified by defining an *average roughness height*, defined as the peak-to-trough distance. They found that in general, coarser grains which presented higher roughness levels (37 to 74 μm) present greater closure levels (K_{clos}/K_{max} = 0.5 to 0.7). Ohtsuka[15] found considerable sliding effects at low stress intensities and K_{open}/K_{max} values as high as 0.8 in 1018 steel. Suresh[9] studied fatigue crack growth in duplex microstructures with ferrite and martensite and found that when ''chunks'' of martensite existed in the ferrite phase the crack paths were highly nonlinear. He noted that both the crack surface interference effects and crack deflection from a planar path contribute to the fatigue crack growth resistance. Minakawa and McEvily[16] reported very high closure levels ($\approx$0.75) and sliding of crack surfaces in ferritic-martensitic 1018 steel with considerable asperity-induced crack closure.

The preceding considerations of the literature demonstrated that asperity-induced closure can develop when the height of the asperities is comparable to the crack opening displacement (COD). Since the COD in cyclic loading is of the order of microns, it is not surprising that a crack surface roughness of tens of microns can induce considerable crack closure levels. Therefore, this mechanism is expected to be dominant under low ΔK levels and at lower R ratios. When asperity-induced closure occurs, the normal-

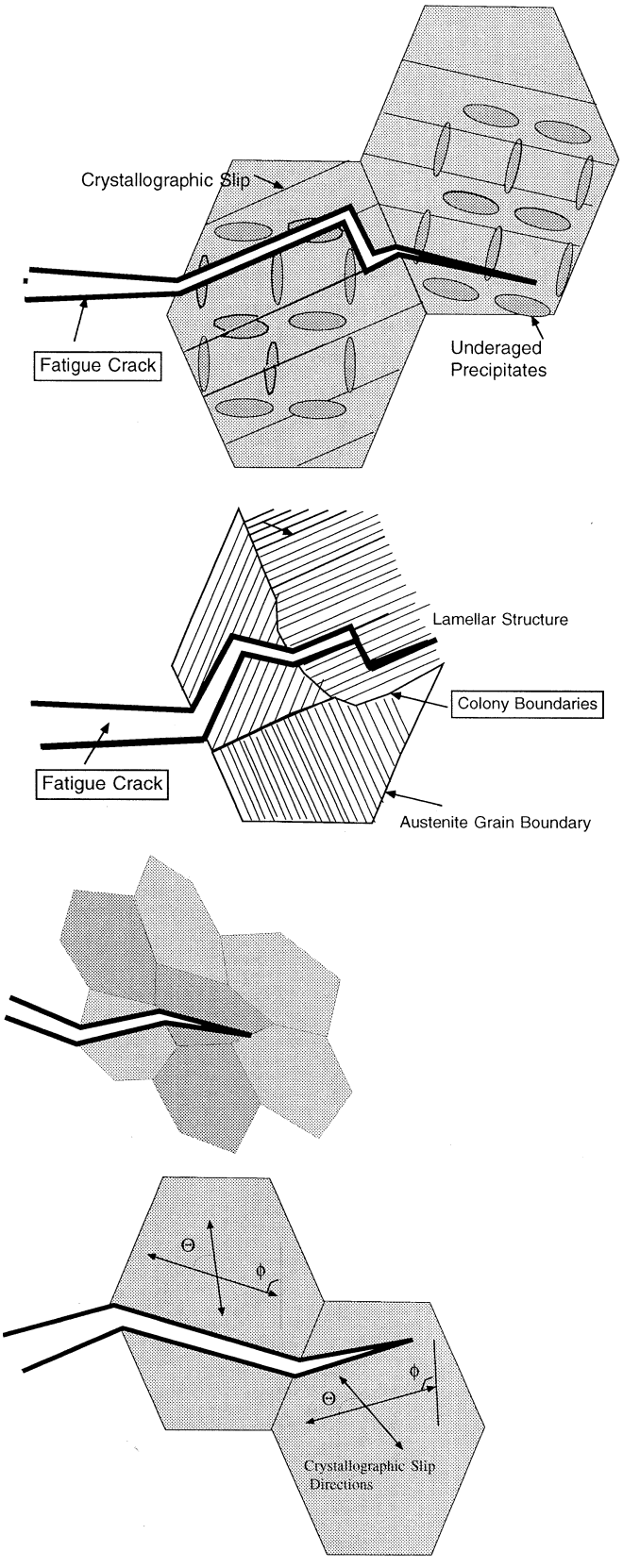

Precipitation Hardened Al alloys
Al-Cu-Li
Al- 2xxx series
Al- 7xxx series

Nickel Based SuperAlloys

Fully Pearlitic Steels
Ti with 4-8 Al
Ti-4Al-6V with acicular structure
TiAl intermetallic alloys

Ferritic-Pearlitic Microstructures
Ferritic-Martensitic Microstructures
Duplex (α and β) microstructure in Ti Alloy

All polycrystalline Alloys with misoriented grains

Fig. 1—Summary of alloy systems where crack paths are nonlinear.

ized opening stress levels often exceed 0.5 and could reach 0.8 in some cases. Since these closure levels exceed the plasticity-induced closure effect ($S_{open}/S_{max} < 0.5$ in most cases), this led to the conclusion that roughness or asperity-induced crack closure is the main closure mechanism in the near-threshold regime.

The present model aims to quantify the closure of surfaces due to irregular crack paths without introducing plasticity- or oxide-induced crack closure. The stress intensity factor levels will be low ($K_{max} < 20$ MPa$\sqrt{m}$), such that they characterize the threshold region. It is important to note that at small stress intensities, the plastic zone size is smaller than the grain dimensions or the microstructural element relevant to crack advance. In the majority of cases chosen, including both R ratios of 0.1 and -1.0, the crack tip opening displacements will be lower than the roughness heights, and the role of crack closure will be significant.

II. MODELING CAPABILITIES

A. *Topographical Parameters*

Traditionally, when quantifying the effect of roughness on crack growth, only one topographical parameter is accounted for. This parameter, which is usually directly related to the height of the asperities, provides a one-dimensional description of the fracture surface. In the present development, the equivalent parameter is the standard deviation of heights (σ_0). The closure effect observed during the simulations is highly dependent on this variable. However, results are also sensitive to other surface parameters. These describe the surfaces by quantifying the radii of the asperities (*i.e.*, profile) and the dispersion of asperities (*i.e.*, their frequency of occurrence). The three topographical parameters which enter in the computation of the opening levels are illustrated in a ''strip'' in Figure 2. Many such strips are assumed (>50) over the fracture surface. For simplicity, three asperities are shown with radii R_1, R_2, and R_3, respectively. The height of each asperity is denoted as z_1, z_2, and z_3. The density of asperities per unit length is denoted as N, which is $1/n$, where n is the number of asperities per unit length.

The initial standard deviation of asperity heights (σ_0) is assumed to be the same for the two contacting fracture surfaces. This accounts, to some degree, for the fact that the surfaces present similar degrees of roughness. We take a reference, or datum, at $z = 0$ such that the mean is zero, so σ_0 is a function of the height z given by

$$\sigma_o = \left[\frac{\sum_i^n z_i^2}{n - 1}\right]^{1/2} \quad [1]$$

where n is the total number of asperities.

The density of asperities (N) is assumed to remain constant over the crack dimension. Here, we assume that as the separation distance decreases, some asperities are flattened but new ones are formed as the crack advances. The range considered is 10 to 1000 asperities/cm. The initial, undeformed radius of asperities tips (R_0) is also assumed constant. This also represents an idealization, since in real fracture surfaces the radius of the asperity tips might also vary randomly. Since topographical variables must be physically consistent, relationships can be established to ensure this consistency. The average roughness is in the range of 0.1 to 100 μm. The surface density of asperities refers to the size of an asperity (Figure 2); for a given profile, the higher the density, the lower the width of the asperities. In the development of the unit event (Part 1 of this article), it was assumed that each asperity is cylindrical; therefore, we idealize the cross section of a fracture surface as being topped with two-dimensional rounded asperities. The width of each asperity, as defined in Figure 2, must be larger or, at most, equal to the diameter of the circular cap. That is,

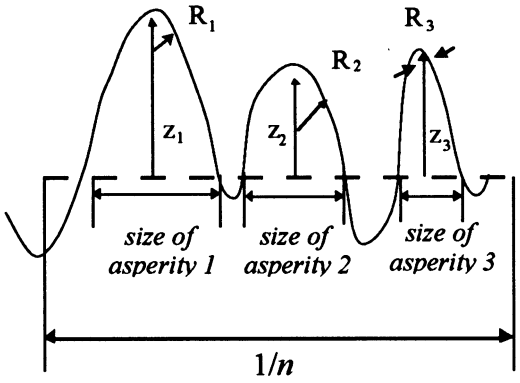

Fig. 2—Illustration of topographical parameters including asperity heights, asperity radii, and asperity density.

$$\frac{1}{N} \geq 2R_o \quad [2]$$

where N is the number of asperities per unit length. For example, if there are 100 asperities/cm, then the largest average asperity size can be deduced by looking at the limiting case when the asperities are closely packed and there are no gaps between them. Then, an asperity will take up 0.01 cm or 100 μm. Therefore, the radius of this asperity can be as large as 50 μm but not higher.

In order to eliminate one of the topographical variables and to isolate the effects of the others, a relationship between R_0 and N was assumed:

$$\frac{1}{2.2N} = R_o \quad [3]$$

This makes a statement about the dispersion and shape of asperities along a cross section. The result is a fairly dense surface. Even though this ''average'' shape is thought to be roughly representative of fracture surfaces, it is noted that this choice is not necessary. It is arbitrary and made for the sole intention of studying the effect of specific topographic characteristics that are of more interest to this application. Beyond the relationship between R_0 and N, the choice of s_0 is arbitrary. The height-to-size ratio (σ_0/R_0), along with material properties, governs the mode of asperity deformation.

In their study of contact, Kapoor and Johnson[17] defined the σ_0/R_0C ratio as a measure of plastic deformation. As this ratio increases, so does the number of contacting asperities which are plastically deformed. At $\sigma_0/R_0C > 100$, most asperities are plastically deformed in the first few cycles. When this ratio is small ($\sigma_0/R_0C < 50$), most asperities are elastic at low load, but as load increases, more and more plastically deform and achieve shakedown. This ratio is a function of surface topography and material properties by the constant (C), which is given by

$$C = \left[\frac{p_o^s}{E^*}\right]^2 [2 \ln (4E^*/p_o^s) - 1] \quad [4]$$

where p_0^s is the Hertzian contact pressure at shakedown and E^* is the plane strain elastic modulus. The p_0^s term will be explained in detail in Section II.B. The value of C is the ratio of deformed interference to the deformed radii of asperities in the shakedown state. However, due to the assumption of constant maximum pressure at shakedown, it is dependent only on the material properties E and k (through the p_0^s/k ratio), making C a measure of deformation independent of topographical parameters. It is advantageous to have such a parameter that can be uniquely defined for a given material. The ratio σ_0/R_0 corresponds to, in the case of R_0/N remaining constant, a sense of height *vs* size and fully encompasses the effect of the surface's topography.

B. *The Role of Shear Tractions or Friction*

The shear-to-normal load ratio in contact with two surfaces is termed the ''traction coefficient.'' In crack contact, the shear loading can be present due to far-field mode II loading and also due to friction effects in the absence of remote shear loading. In the present case, the regimes of operation for two contacting bodies are shown in Figure 3(a).[18] The geometry of the contact is also shown in the right-hand side of the figure. In this figure, x is the crack growth direction and y is the thickness direction. The Hertzian pressure integrated over the contact width ''$2x_h$'' results in the total normal load (P) and shear load (Q). The applied contact stress factor is defined by p_0/k, where p_0 is the peak pressure in Hertzian contact (which has the elliptical shape) and k is the yield stress in shear. Curve A is the elastic limit (*i.e.*, the first yielding). If the operating pressure and shear tractions fall below curve A, the material never yields. Curve B is the shakedown limit. It is higher than the elastic limit, especially at small values of traction coefficient. If the operating point is between lines A and B, the material will yield in the first loading but then becomes elastic in subsequent loadings. Line C represents the shakedown limit for a kinematically hardening material. Above line C, the material undergoes ratchetting (accumulation of strain each cycle) which leads to directional plastic flow. Note that curves B and C coincide at high values of traction coefficient corresponding to plastic flow on the surface. When the traction coefficient is lower, the plastic flow occurs subsurface and the curves B and C diverge. In the present work, we are concerned with contact of asperities such that shakedown occurs. The shakedown is achieved because the profile of the asperities is modified under the plastic flow and, in the limit of the contact region, experiences a constant shakedown pressure (p_0^s/k) during the contact period. In the analysis of Johnson and Schercliff,[18] the shakedown limit shown in Figure 3(a) was assumed to hold between the two asperities. Clearly, if the geometry of contact changes from the cylindrical plane strain contact situation used in the derivation of Figure 3(a), the results need to be modified. Nevertheless, Figure 3(a) with curve C can be used as a first approximation of the interaction of two asperities.

The tangential-to-normal load ratio (Q/P) enters the analysis because it changes the shakedown pressure to shear yield stress ratio (p_0^s/k) along curve C. This ratio depends on the choice made for the shakedown map. This, in turn, is dependent on the geometry of the unit event problem. The simulations were conducted for two cases. In the first case, $p_0^s/k = 4.0$, corresponding to a traction coefficient of zero. However, when shear tractions were present ($Q/P > 0$), the value of p_0^s/k decreases to a value less than 4.0. Therefore, for the second case, the value $p_0^s/k = 2.5$ was used, which corresponds to a traction coefficient (Q/P) of 0.4.

Note that the accuracy of Figure 3(a) has been checked with finite-element study of rolling/sliding contacts[19] and the agreement has been satisfactory. Also, more sophisticated constitutive models[20] have been used, which allowed further refinements to the rolling/sliding contact problem. The work of Sehitoglu and his students focused on how many cycles elapsed before the stress-strain response undergoes shakedown. For the purposes of the current study, the results in Figure 3(a) are acceptable because they produce shakedown conditions without specifying the transient changes in deformation behavior.

A schematic of the change in profile of the asperities due to plastic deformation is given in Figure 3(b). Both crack surfaces are shown in this figure at far-field stress levels below the opening stress. The arrows denote material that has been permanently compressed due to sliding of the surfaces. It is assumed that the asperities change their profile to assume the constant value of p_0^s.

III. RESULTS OF SIMULATIONS

A. *Present Model Simulations*

The material properties used in the simulations (Table I) correspond to γ-TiAl (for more details on this material, refer to Balsone *et al.*[21]); however, normalization permits applicability to other materials. The variables can be grouped into three categories: topography, material properties, and loading conditions (Table II). The effect of each was isolated by keeping all other parameters constant. We note that the topography is characterized by N and σ_0, the lateral tractions or friction effects are governed by p_0^s/k, and the remote loading conditions are the maximum stress and R ratio and the initial values of stress intensity and crack length.

In the model simulations, the crack grew under far-field mode I loading conditions. By changing the Q/P ratio it is possible to simulate the effect of far-field mode II loading or the effect of friction. At the local level, sliding displacements were present. Simulations were conducted for a systematic variation of conditions. In most cases, a crack was propagated through 100 loading cycles. For most results presented, the initial crack length (c_i) was 100 μm and the final crack length (c_f) was 1000 μm. The initial maximum stress intensity varied between 1 and 5 MPa$\sqrt{\text{m}}$. The final maximum stress intensity varied between 10 and 20 MPa$\sqrt{\text{m}}$.

B. *Effect of Standard Deviation of Heights, S_{max}/S_y, and p_0^s/k*

The effect on the crack opening stress levels of varying the standard deviation of heights (σ_0) and $S_{\max}/S_y$, while fixing the remaining variables, is displayed in Figures 4(a) and (b). For each of these simulations, three different values of the initial standard deviation of asperity heights, holding all other topographical parameters constant, were consid-

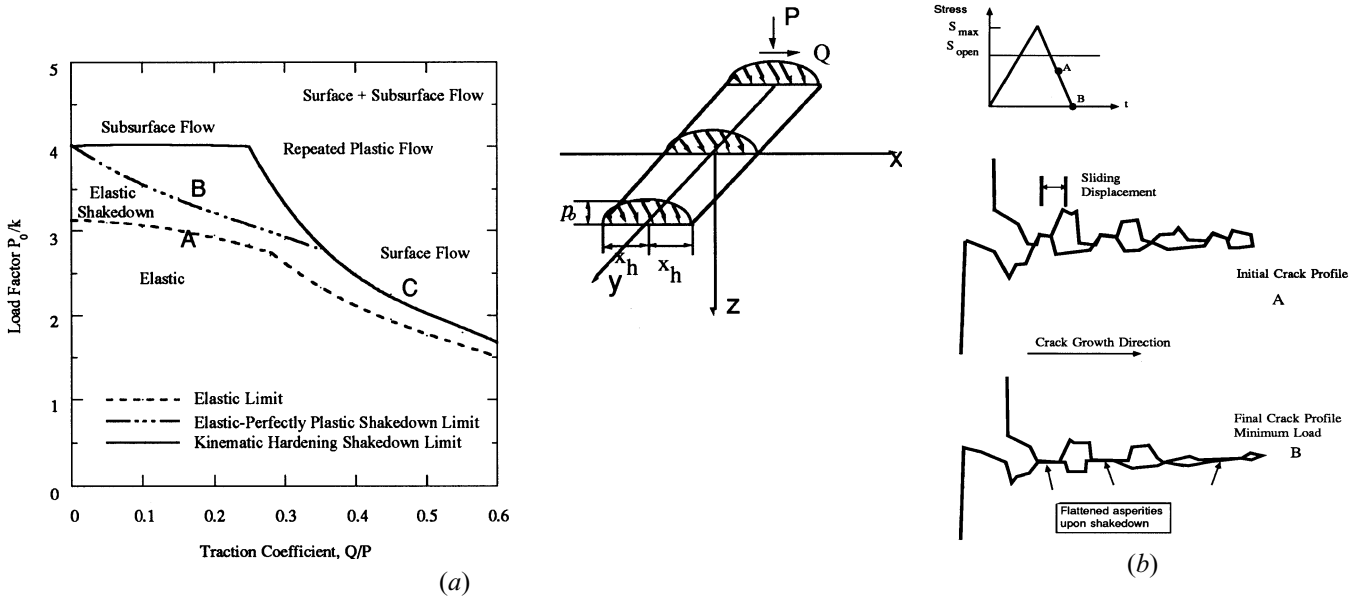

Fig. 3—(*a*) Normalized peak Hertzian pressure *vs* the traction coefficient displaying the different operating regimes. The curve relevant to the current study is the ''elastic shakedown.'' (*b*) Schematic of crack surfaces before crushing of the asperities and after shakedown (or flattening of the asperities). Note that there are multiple contact regions and gaps behind the crack tip.

ered. In the case of Figure 4(a), the crack grew such that initial stress intensity of 3.9 MPa$\sqrt{\text{m}}$ increased to a final stress intensity of 13.2 MPa$\sqrt{\text{m}}$. Each curve reflects the decrease in the opening levels during the progression of a fatigue crack over 100 cycles with a maximum stress of 270 MPa ($S_{max}/S_y = 0.6$). In Figure 4(b), $S_{max}/S_y = 0.2$ was considered. From these figures, a clear sensitivity to variations of σ_0 and S_{max}/S_y is demonstrated. In all figures, an increase in σ_0 leads to an increase in S_{open}/S_{max}. Three values of σ_0 (1, 10, and 40 μm) were considered in the simulations. Values of σ_0 outside these bounds will be given later. In Figure 4(a), a 10 times increase in σ_0 leads to a factor of 3 increase in opening levels. However, the increase is even larger when changing from 10 to 40 μm. This sensitivity varies in all the opening *vs* crack length figures. Other parameters influence the results and are responsible for this variation. For the case of $\sigma_0 = 40$ μm and $S_{max}/S_y = 0.2$, the crack opening stress level was at 1.0. Note that the asperity density (N) is maintained constant in all simulations at 100 asperities/cm and the R ratio in the simulations was 0.1. The initial (undeformed) roughness was maintained ''constant'' as the crack progressed. If the roughness level (σ_0) was allowed to decrease along the crack length, the transient opening stress level *vs* crack length curves shown in Figures 4(a) and (b) would be steeper. This will be discussed later when comparing simulations with TiAl closure data.

The role of p_0^s/k on the crack opening simulations is given in Figures 4(c) and (d). In these cases, the p_0^s/k value was maintained at 2.5. This ratio can be interpreted in the following way. In the presence of local friction between the contacting surfaces, the normal pressure at shakedown decreases to levels below the $p_0^s/k = 4.0$ value. In the case of $Q/P = 0.4$ (lateral force 40 pct of the normal force), the shakedown pressure is $p_0^s/k = 2.5$ (Figure 3(a)). Another way to interpret the $p_0^s/k = 2.5$ case is to view the Q/P ratio of 0.4 as far-field mode II loading, such that the mode II component is 40 pct of the mode I component. In the case of $p_0^s/k = 2.5$, the crack opening stress levels are lower than the $p_0^s/k = 4.0$ case for both $S_{max}/S_y = 0.2$ and 0.6. The results suggest that in conditions where the tangential load contribution is greater, the surface's topography will require less of a normal load to be flattened and permanently deformed. This idea was also explored in Part 1 of this article, when several models for contact between random surfaces were compared.

Table I. Material Properties Used in Simulations Shown in Figures 4 through 7

Variable	Value Used in Simulations
Elastic modulus, E	180 GPa
Plain strain modulus, E^* $\left(E^* = \frac{E}{2(1-\nu^2)}\right)$	98.9 GPa
Poison's ratio, ν	0.3
Yield stress, S_y	450 MPa
Yield stress in shear, k $k = \frac{S_y}{\sqrt{3}}$	261 MPa

Although in the simulations the p_0^s/k ratio were held constant over the cycling, it is reasonable to expect that in real situations this might not be the case. It is expected that due to the change in asperity profiles, the formation of wear debris, and changes in surface due to environment, this coefficient may change. Furthermore, if cyclic hardening (increase in strength induced by cycling) of the material is taken into account, then k would increase. It is expected that the low sensitivity to crack length seen in the opening level *vs* crack length plots results from, among other factors, assuming unchanging tangential-to-normal traction (Q/P) conditions through cycling.

Higher opening levels with decreasing S_{max}/S_y were observed, and this effect is mainly due to the fact that the separation distance decreases with this ratio. Lower values

Table II. Parameters Varied during Simulations (Figures 4 through 7)

Category	Variable		Range of Values
Topography	Surface density of asperities	N	10 to 1000 asperities/cm
	standard deviation of heights	σ_0	0.1 to 120 μm
Lateral traction ratio (Q/P)	shakedown pressure to shear yield stress	p_0^s/k	2.5 ($Q/P \sim 0.4$), 4.0 ($Q/P \sim 0.0$)
	maximum stress to yield stress ratio	S_{max}/S_y	0.2, 0.6
Remote loading conditions	minimum stress to maximum stress ratio	R ratio	0.1, -1
Initial conditions	Initial stress intensity		1 to 10 MPa $\sqrt{m}$
	initial crack length		10 to 1000 μm

of S_{max}/S_y also correspond to smaller plastic zone sizes ahead of the crack tip. The size of the plastic zone is an indicator of how much plasticity-induced closure may be occurring at a given stage of crack growth. The results are consistent with the hypothesis that in the near-threshold (small plastic zones) regime, the contribution to closure is primarily due to crack surface interference.

C. *The Effect of Asperity Density (N)*

All the previous runs were conducted under $N = 100$ asperities/cm conditions. To gain further insight into the effect of asperity density effects on crack closure, simulations were conducted for the case of $N = 10$ and 1000 asperities/cm. The results are shown in Figures 5(a) and (b). The σ_0 values were maintained as before, except in Figure 5(b), where $\sigma_0 = 0.1$ μm was included. We note that the asperity density has a considerable influence on the crack opening stress levels, especially for $N = 100$ and 1000 cases. In the case of $N = 1000$ asperities/cm, the $\sigma_0 = 40$ μm would predict that the crack is completely closed during the cycle; hence, this result was not included. We note that in the analysis of contact, we assumed a constant asperity density all along the crack length. If the asperity density is a function of crack length this can be handled in the analysis, but this was not considered.

D. *Crack Opening Displacements*

It is useful to gain further insight into results by comparing the surface roughness (σ_0) with the COD. Specifically, we will compare the crack opening stress levels with respect to the normalized COD/σ_0. The COD is given by following formula:

$$\text{COD} \approx \frac{K_{max}^2}{S_y} \frac{(1 - \nu^2)}{E} \quad [5]$$

where E is the elastic modulus and S_y is the yield stress. Detailed finite-element analysis predicts that the actual crack tip opening displacement is smaller than Eq. [5], but for our purpose, it is used as a scaling factor.

The results are displayed in Figure 6, which was obtained by compiling data for three different values of N but holding all other variables constant. The results from $S_{max}/S_y = 0.2$ and 0.6 are superimposed in Figure 6 with remarkable agreement. Therefore, Figure 6 can be used as a closure ''map'' to handle a variety of cases, but one should be cautious not to overextrapolate the results. In the construction of this map, the opening values were obtained for cycle number 50 where the crack length is about 600 μm. Figure 6 shows the decrease in closure levels as the COD increases. The horizontal axis is presented as log scale because the COD/roughness can vary by four orders of magnitude. Since CODs are of the order of microns and the roughness can be tens of microns, premature of closure of crack surfaces readily when COD/$\sigma_0 < 1$. As expected, the curves collapse as COD/σ_0 increases and reaches the $S_{open}/S_{max} = 0.1$ limit. However, the assumption of a Gaussian distribution of heights implies that there will always be a probability of contact. Similar trends to the results in Figure 6 develop when tangential tractions are present and, also, similar trends exist for $R = -1$ conditions. The results in Figure 6 can be described by an equation of the following form:

$$\frac{S_{open}}{S_{max}} = A + B \cdot \left(\frac{\text{COD}}{\sigma_o}\right)^C + D \cdot \exp\left(-4 \cdot \left(\frac{\text{COD}}{\sigma_o}\right)^{0.8}\right) \quad [6]$$

where A, B, C, and D are constants. For the $N = 100$ asperities/cm case, $A = 0.028$, $B = 0.17$, $C = -0.225$, and $D = 0.066$. For the $N = 100$ case, the equation can be used in the range of COD/σ_0 from 0.001 to 40. We note that rapid changes in S_{open}/S_{max} occur when COD/σ_0 is less than 1. For the case of $N = 10$ asperities/cm, the constants in Eq. [6] are $A = 0.025$, $B = 0.105$, $C = -0.22$, and $D = 0.05$. With these constants, the equation can be used for COD/σ_0 in the range of 0.0001 to 4. These constants and Eq. [6] allow the results presented in Figure 6 to be correlated closely.

E. *σ_0/R_0C and R Ratio*

In Figure 7(a), the crack opening stress levels are shown *vs* the nondimensional ratio (σ_0/R_0C) for the $R = 0.1$ case. The trends suggests that if C is constant (and, thus, for a given material), increasing the σ_0/R_0 ratio will increase the opening loads. Again, this results from the fact that as the σ_0/R_0 ratio increases, a greater number of asperities will make contact; this describes a shape that governs plastic deformation. As σ_0/R_0C increases, the crack opening stress

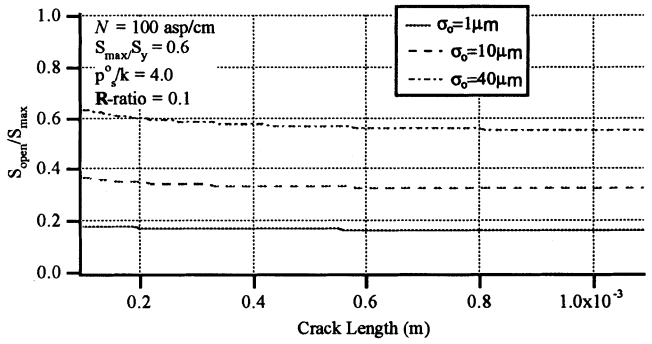

(*a*)

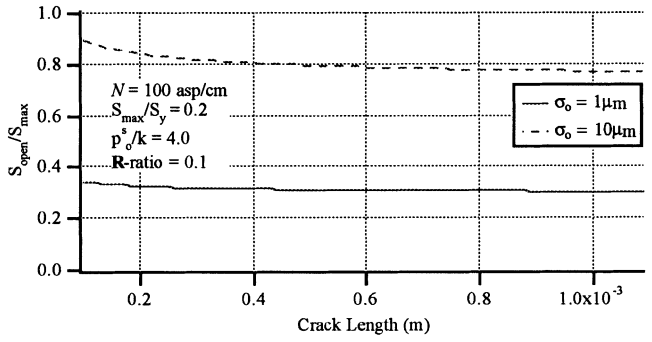

(*b*)

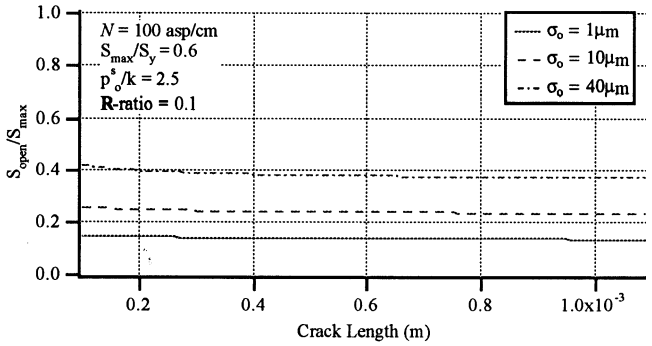

(*c*)

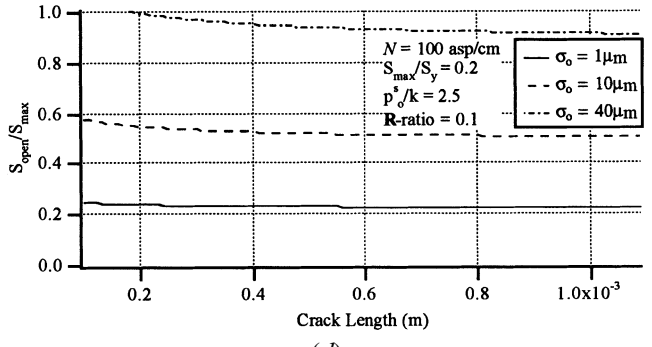

(*d*)

Fig. 4—Normalized crack opening stress *vs* crack length for varying S_{max}/S_y ratio and $p_0^*/k = 4.0$ ((*a*) and (*b*) no shear tractions) and $p_0^*/k = 2.5$ ((*c*) and (*d*) with shear tractions).

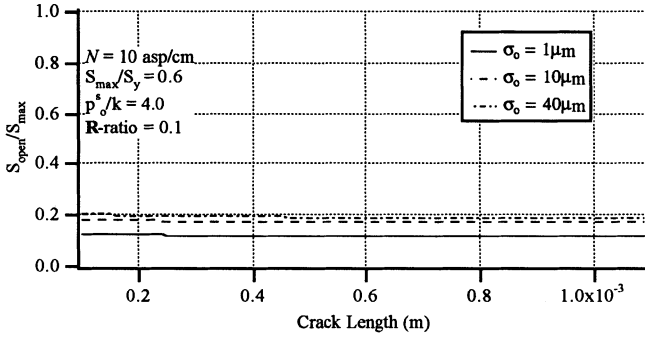

(*a*)

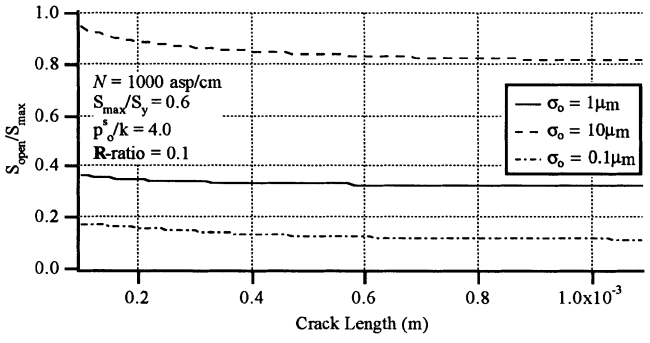

(*b*)

Fig. 5—(*a*) and (*b*) Normalized crack opening stress *vs* crack length for varying asperity density, *N*.

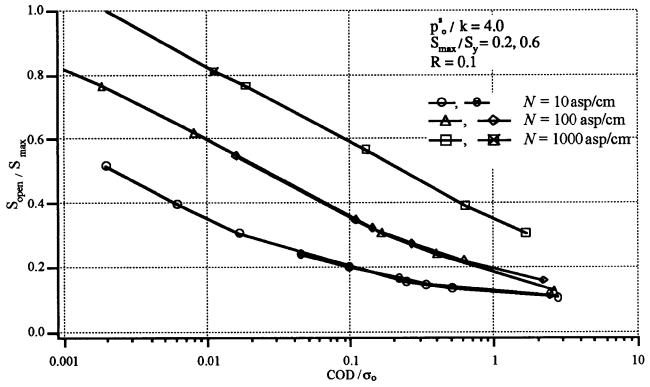

Fig. 6—The variation of S_{open}/S_{max} as a function of normalized COD. Note that the results from $S_{max}/S_y = 0.2$ and 0.6 cases are in close agreement.

levels increase in a nonlinear fashion. If the ratio is small, not only will the number of contacts be fewer, but the load will be carried elastically and the opening levels will be lower. Note that Figure 7(a) can be interpreted as an opening stress *vs* roughness plot. For a material with $k = 261$ MPa and $E^* = 99{,}000$ MPa, the value of C is 0.0003026 and, given R_0 as $1/2.2N$, the product R_0C is 0.137. The x axis spans from 5 to 1000 in Figure 7(a); the 1000 corresponds to a roughness of 137 μm while 5 corresponds a roughness of 0.7 μm. We note that the opening stresses are considerably greater with $S_{max}/S_y = 0.2$ than with $S_{max}/S_y = 0.6$. Note that as $\sigma_0/R_0\ C$ approaches 5, the crack opening stresses approach the minimum stress (*i.e.*, $S_{open}/S_{max} \rightarrow 0.1$). The effect of material strength enters the calculation in two places: it affects the S_{max}/S_y value and also the C parameter. We note that the sensitivity of the results to applied maximum stress is far more significant than that observed in the well-studied plasticity-induced closure. In plane strain, the plasticity-induced closure is not a strong function of S_{max}/S_y, particularly when $R > 0$.

The effect of $R = -1$ is shown in Figure 7(b). In this case, the horizontal axis σ_0/R_0C also spans the range of 5 to 1000. The results indicate that for the $R = -1$ case, the

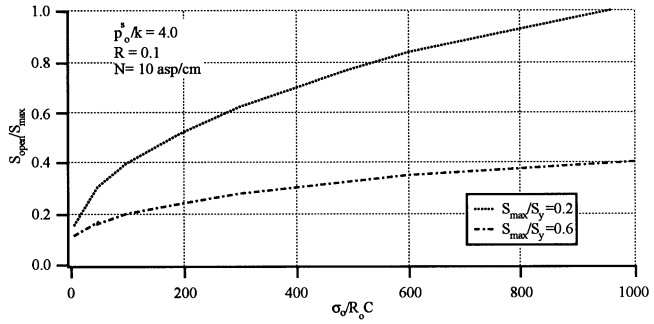

(*a*)

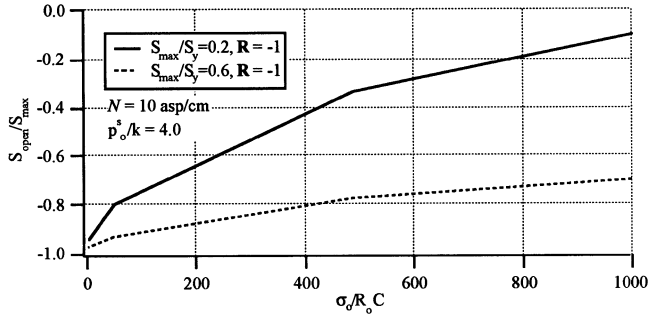

(*b*)

Fig. 7—(*a*) Variation of opening levels under $R = 0.1$ with increasing roughness. (*b*) Variation of opening levels under $R = -1$ with increasing roughness.

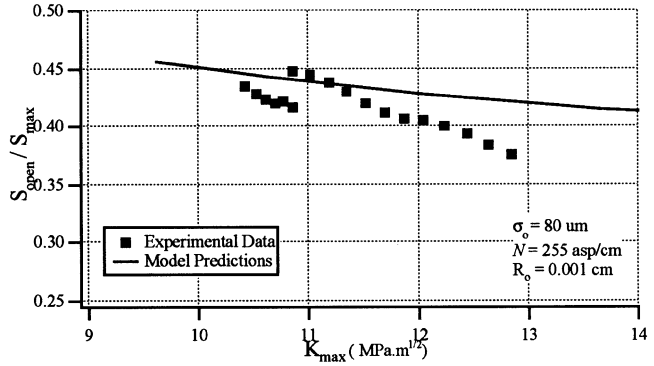

Fig. 8—The decrease in normalized crack opening stress with crack growth displaying the experimental and predicted trends on γ-TiAl aluminide with lamellar microstructure.

crack opening stress levels are below zero, which means that cracks open when the far-field stress is in compression. For the case of $S_{max}/S_y = 0.6$, the normalized crack opening stress is in the range of -1.0 to -0.75, while for the $S_{max}/S_y = 0.2$ case, the normalized opening stress levels span a wider range, namely, -1.0 to -0.2. Note that as σ_0 approaches 0 in the $R = -1$ case, S_{open}/S_{max} approaches -1, as expected. We note that the corresponding crack opening stress levels for plasticity-induced closure are higher than those shown in Figure 7(b).[22]

IV. COMPARISON WITH EXPERIMENTAL OBSERVATIONS

Although asperity-induced crack closure has been recognized for some time, it is not customary to include topography information along with fatigue crack growth results. In the current work, we have analyzed TiAl specimens that were tested at Wright-Patterson Air Force Base (WPAFB), in detail. Both the crack growth rate and crack closure level were measured in these tests. The fracture surfaces were then quantified using confocal microscopy.

A. *γ-TiAl*

This material is being developed for high-temperature application in gas turbines. Heat treatments can produce a fully lamellar structure (grains of $\alpha_2 - \gamma$ lamellae) or a duplex microstructure (equiaxed γ and lamellar grains). The composition of both alloys is Ti-46.5Al-3Nb-2Cr-0.2W. The fatigue crack growth resistance of the lamellar alloy is superior to the duplex microstructure, and the ΔK_{th} obtained under $R = 0.1$ conditions was 6 MPa$\sqrt{m}$ for the duplex microstructure and 8 MPa$\sqrt{m}$ for the lamellar case. Both microstructures of γ-TiAl (both the fully lamellar and duplex structures) exhibit rough crack paths and some experimental crack closure data has been documented. In fact, in the alloy studied, asperity-induced closure is responsible for dependence on microstructure, which resulted in a superior growth resistance in a lamellar (rougher) microstructure to that of a duplex microstructure. The material properties of this alloy are presented in Table I.

A fractographic analysis showed that alloy exhibiting a lower roughness level (such as the duplex microstructure) had close-to-Gaussian asperity height distributions, whereas for the lamellar case (which had a wider variation in asperity sizes and heights), the variation in asperity heights did not conform well to a Gaussian distribution. The experimental results displayed in Figure 8 are for a fully lamellar microstructure under $R = 0.1$ conditions. The fractographic analysis for this microstructure predicted a range of root-mean-square of height values between 75 and 150 μm. The simulations used the following values: $\sigma_0 = 80$ μm and $R_0 = 1/(3 \cdot 9 \cdot N)$, where $N = 25.5$ asperities/cm. An initial Gaussian distribution of heights and $p^s_0/k = 2.5$ was assumed. The experimental crack closure levels were obtained by Dr. Brian Worth (WPAFB). The model estimates are fairly accurate, specially at the lower-K end, but as K increases the model fails to predict a sharp decrease in opening levels. This is partly because we assumed a uniform roughness profile as the crack grew; in reality, the roughness will decrease, resulting in a rapid decrease in crack opening stress.

B. *Comparisons with Other Experimental Results*

It is possible to use the results of this study to estimate closure levels for different materials. Allison and Williams[23] measured closure levels in TiAl alloys with Al contents of 4 and 8 pct and also studied the role of aging. They found normalized closure levels as high as 0.74 (Ti-4Al) for a maximum asperity height of 70 to 80 μm and higher values for the Ti-8Al alloys. The roughness variations in these alloys are related to the change in slip character from wavy to planar with increasing Al content and with aging. Experimental and predicted results are compared in Figure 9. For all materials examined, the roughness values exceeded the crack tip opening displacement by orders of magnitude. This parameter was determined by profilometric measurements. If we estimate the standard deviation of a

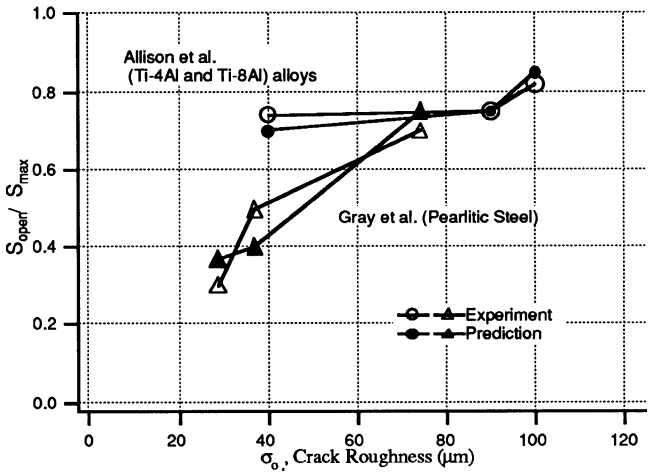

Fig. 9—Comparison of experimental and predicted normalized crack opening stress levels as a function of roughness.

surface to be half of the maximum asperity height, we can use Figure 7(a) (assuming no friction and $S_{max}/S_y = 0.2$) to estimate closure levels for this material. By accounting for the material properties in the coefficient C, and assuming $N = 30$ asperities/cm (since the roughness is very high, a low density of asperities makes physical sense), we can calculate the σ_0/R_0C ratio. These results are presented in Figure 9.

Similarly, comparisons can be made to Gray *et al.*'s[8] work on pearlitic 1070 steel. In this class of alloys the microstructure is lamellar, as shown in the schematic of Figure 1(a). Depending on the prior austenite grain size, pearlite colony size, and interlamellar spacing, the crack growth rates and threshold stress intensity range vary. The experimental crack closure levels shown in Figure 9 were obtained for the same alloy but under different heat-treatment conditions. By taking $\sigma_0 = 37$ μm and $N = 10$ asperities/cm, then $\sigma_0/R_0C = 612$ and $S_{max}/S_y = 0.4$, the simulations shown in Figure 9 were obtained. Again, the agreement with experimental data is satisfactory.

The results are in general agreement with the experimental findings of Ritchie *et al.*[4] on 2124 aluminum alloys. They found that in the underaged case, ΔK_{th} was 3.58 MPa$\sqrt{m}$ and measured a normalized closure level of 0.65. Their finite-element results of plasticity-induced closure resulted in a normalized closure level of 0.25 and consistently underpredicted the experimentally observed closure levels. They correctly noted that the role of crack surface interference provided significant additional closure. The concepts developed in this article can be invoked to address the experimental results of Ritchie *et al.* Using $\sigma_0 = 10$ μm, COD/ σ_0 of 0.063, and an asperity density of 100 asperities/cm, we predicted (using Figure 6) a normalized closure level of 0.65, which is in perfect agreement with experimental results. In the same work, Ritchie *et al.* noted that for naturally occurring small cracks (2 to 400 μm), the asperity-induced closure develops due to interactions with the microstructural constituents. Since these cracks are driven at higher S_{max}/S_y ratios compared to threshold testing, the normalized closure levels are expected to be lower. Consequently, cracks grew at a stress intensity range of 0.9 MPa$\sqrt{m}$, well below the threshold.

Bao and McEvily[24] studied 9Cr-1Mo steel in compact tension (CT) specimens of 6.35 mm thickness. As the crack grew from 6.8 to 26 MPa$\sqrt{m}$, the normalized crack opening stress level decreased from 0.44 to 0.16. McEvily[25] measured the average height of the asperities and reported 2.5 μm for this entire range of crack growth. It is possible to estimate these results based on Figure 6. This material has a yield strength of 531 MPa. The COD/σ_0 value calculated for the initial stress intensity of 6.8 MPa$\sqrt{m}$ was 0.16, and for 26 MPa$\sqrt{m}$ the COD/σ_0 ratio was 2.36. Assuming nearly 500 asperities/cm (1 asperity/20 μm), the corresponding normalized opening stress levels are 0.4 and 0.2, respectively. This compares favorably with experimental normalized opening stress levels of 0.44 and 0.16.

V. DISCUSSION OF RESULTS

A model for the prediction of asperity (roughness)–induced crack closure due to nonflat crack surfaces has been developed, using the statistics of rough surfaces and contact mechanics to characterize the stresses due to interference. The model estimates crack opening stress levels for a propagating fatigue crack under a variety of far-field loading and local geometric conditions. The results are presented in normalized form for most cases, but they can be denormalized to suit specific applications.

The present model overcame several limitations of the previous models in the study of closure in the near-threshold region. The effect of multiple asperities was accounted for by considering different values of the surface asperity density. The model allows for many contact points behind the crack tip. This is an advantage over discreet asperity contact models. Plastic flow of asperities was accounted for in the analysis. The three-dimensional stress field generated due to asperity contact is inherent in the model. The model can handle negative and positive R ratios and the permanent change in profile under different R-ratio conditions. A random profile of asperities was studied and the fractography study on the titanium aluminides confirmed that fracture surfaces conform to a random profile and cannot be described by an idealized geometric profile.

We note that the results can explain several phenomena observed experimentally that have not been fully understood. Early finite element modeling (FEM) results on plasticity-induced closure showed that under plane strain closure conditions the crack opening stress levels were as low as 0.3 (*i.e.*, $S_{open}/S_{max} = 0.3$) at low levels of far-field loading ($S_{max}/S_y < 0.2$), and the opening stress levels approached the minimum stress as the S_{max}/S_y levels exceeded 0.6. This has led some investigators to ignore crack closure under plane strain conditions or argue that it cannot be a significant factor in plane strain. The present results show that crack closure due to asperities (Figure 7(a)) can be significant when the roughness levels exceed $\sigma_0/R_0C = 50$ under $S_{max}/S_y = 0.2$ conditions. In fact, the magnitude of crack opening stress reaches its maximum when $\sigma_0/R_0C > 900$. Therefore, the asperity-induced closure can explain the R ratio, S_{max}/S_y, and crack length effects even when the plasticity-induced closure effects are arguably small.

Many of the transient effects which result from cyclic loading are accounted for in the model. For example, in the construction of the load-separation distance relationship[3] asperity profile changes due to repeated contact were in-

cluded. However, as the crack grows through the microstructure and the crack paths become more linear, the statistics of the crack surface may change, *i.e.*, the distribution of the asperity heights will be modified. Considering the sensitivity of the load-separation distance behavior to the change in distribution (Figure 6),[3] the effect on the results could be important. Therefore, the predicted decrease in opening stress levels with crack length is not as dramatic as experimental trends (Figures 4, 5, and 8). Another history effect that was not accounted for is the change of the Q/P ratio as a result of cyclic loading. In the presence of constant far-field shear tractions, it is likely that the friction characteristics of the surfaces will change with to and fro cycling and exposure to environment. The model has the flexibility to handle the variation of local traction conditions, but this is left for future experimental and analytical work.

Whether or not the contact loads are supported elastically or plastically in the first few cycles has an important effect on closure levels. There are three possibilities. First, if the surface is readily deformed (soft material and sharp asperities) the deformation will be plastic immediately. These initial contact stresses will be high and, thus, high opening stress levels will result, followed by shakedown where local contact stresses no longer change with cycles. Second, the other extreme of this case would be continuous plastic deformation and ratchetting of the asperities (*i.e.*, no shakedown is achieved; therefore, the present model would be very approximate). This case is anticipated under very high traction coefficients and under high crack growth rates, where steady state or shakedown stress fields are not achieved. Third, in the case of hard asperities with little sharpness (*i.e.*, σ_0/R_0C small), the deformation is expected to be elastic, but contact stresses will still develop. However, the overall contact load that is developed in this case is less than that in the case of immediate plastic flow for the same separation distance.[17] Therefore, the crack opening stresses for this case are expected to be lower.

The results point out that it is difficult to estimate the crack growth behavior of an alloy or make comparisons between different heat treatments based on a single parameter, σ_0. We note that the model predicts crack openings stress levels which increase with increasing σ_0, which is universally accepted. But there are other significant parameters such as the distribution of heights (Gaussian *vs* exponential), asperity density, and loading conditions (S_{max}/S_y, R ratio, and Q/P), which are significant and should be considered.

The work shed further light on the conditions of microstructure, material properties, mode of deformation, and topography of fracture surfaces on crack growth behavior. Consequently, the work has important implications in the design of materials with superior fatigue performance. Early research has found that fine-grained materials produced higher fatigue strength. This is counter to the findings that coarse-grained or planar-slip cases (which promote asperity-induced closure) result in higher stress intensity at threshold and improved fatigue crack growth resistance. Since many materials have initial defects which are precursors to crack initiation, and in cases when the component undergoes many cycles under low stress amplitude, there are advantages to enhancing the fatigue crack growth resistance. If the component does not have preexisting defects, then the overall fatigue performance can be governed by crack initiation and, in this case, fine-grained and wavy-slip microstructures are superior.

The work points out that in order to predict fatigue crack growth, especially in planar-slip or coarse-grained materials, it is essential to characterize the topography to a fairly accurate detail. Given the present-day technology of laser confocal microscopes and other resources, this can be accomplished. One of the main advantages of the model is that it can handle hundreds and thousands of asperities on the crack surface. Discretized FEM or finite difference methods can handle only a very small number of asperities because of computer time. This leads to the conclusion that the model presented here might be quite useful, from a practical point of view, in prediction of fatigue crack growth.

The work addresses plane strain deformation which holds for a wide range of fatigue crack growth rates in metallic alloys, especially in the center of thick bodies and in the near-threshold regime. It is possible to extend the work to a plane stress case by modifying the COD relations and the shakedown map illustrated in Figure 3(a). Furthermore, if asperity sliding with a considerable mode III component develops, this will also modify the contact geometry assumed in Figure 3(a). More information on the asperity profiles in the thickness direction will facilitate such analysis.

The work sheds further understanding on the anomalous behavior of small cracks which exhibit higher crack growth rates than the long cracks at the same stress intensities, but as the same time display the R ratio and overload/underload effects typically observed for long cracks. Experimental trends observed in the literature on the R ratio effects and overload effects on small cracks, however, can be rationalized based on asperity-induced closure agreements. Plasticity-induced closure is very small for short cracks when driven at S_{max}/S_y levels at or exceeding 1.0. Two factors play a role in the acceleration of small cracks: first, there is insufficient wake to induce plasticity-induced closure and second, CODs are large due to far-field plastic strains. The application of underloads has been known to accelerate crack growth, and this can be attributed largely to the reduction of interference of crack surfaces.

The model is able to capture the recent experimental trends of McEvily[25] on center crack and CT specimens. McEvily found significant differences in crack growth rates between center crack and CT specimens for the same material. One of the main differences between these two cases is that at the same stress intensity, (K_{max}), the S_{max}/S_y level in the center crack tension specimen can be 4 times higher than its counterpart in the CT case. McEvily concluded that the asperities are crushed more readily in the higher S_{max} case, resulting in faster crack growth rates for the same K_{max} conditions. The present results demonstrate strong sensitivity to S_{max}/S_y, as summarized in Figures 7(a) and (b). Similar arguments pertaining to plasticity-induced closure in plane stress and in plane strain were made by Sehitoglu and his students to explain the effect of S_{max}/S_y on the fatigue crack growth rates.

Finally, a word of caution. The model studied crack growth behavior due to interacting asperities on a nominally

flat crack surface. If considerable deflections occur from the mode I crack path, the crack growth rates should be analyzed using a mixed-mode stress intensity description. In this regard, and Rice Cotterell[26] considered the driving forces on deflected cracks and Suresh[9] applied these results to periodically tilted crack profiles. These modifications, along with asperity-induced contact, will attempt to provide a more complete description of the effects of microstructure on materials fatigue crack growth resistance.

VI. CONCLUSIONS

The major conclusions stemming from this work are as follows.

1. Using a contact mechanics analysis of surfaces with asperities and by varying the asperity heights and asperity densities systematically, it is shown that crack surfaces undergo asperity-induced crack closure. As the remote stress level, S_{max}/S_y, or crack length increases, the magnitude of the normalized crack opening stress decreases. These trends are related to the relative increase in crack tip opening displacement with respect to the height of the asperities. Experimental trends confirm these transient changes in closure levels.
2. The ratio σ_0/R_0C, which accounts for the effects of topography of the surface and shakedown pressure, was varied in the range 5 to 1000 in the simulations. An increase in height and a decrease in asperity tip radius is conducive to increased contact stresses. The corresponding crack opening stresses spanned from minimum stress in the cycle to maximum stress. Once the effective stress intensity range (ΔK_{eff}) is determined from the crack opening stress, a power-law crack growth rate traditionally used for fatigue cracks $\left(\frac{da}{dN} \approx (\Delta K_{eff})^m\right)$ can be utilized for life prediction.
3. The contact pressure at shakedown changes with the contact geometry, material strength, and shear tractions or frictions experienced by the interacting asperities. As the contact pressure for shakedown (p_0^s/k) decreases from 4.0 to 2.5 when Q/P changes from 0 to 0.4, the closure stresses behind are also lowered. Consequently, the far-field stresses overcome the closure stresses earlier in the cycle and the crack opening stress levels decrease with increasing Q/P. The exact variation of traction coefficient as a result of wear debris formation or environment is a fruitful area of experimental research.
4. The model forwarded in this study sets out a rational procedure for estimating crack growth rates, but is not meant to provide the whole answer to the growth of fatigue cracks. An encouraging outcome of the work was that crack opening stress levels obtained under different conditions overlapped when the results were plotted *vs* the normalized crack tip displacements. Simulations of COD/σ_0 in the range of 0.001 to 3.0 provided variations of normalized crack opening stress spanning from 1.0 (crack remains closed during the entire cycle) to 0.1. The ''closure map'' shown in Figure 6 and Eq. [6] can be readily used to assess the contribution of asperity-induced closure under a broad range of conditions.
5. The crack closure trends in steels, titanium alloys, titanium aluminides, and aluminum alloys were predicted accurately with the model. In all cases, the normalized closure levels exceeded 0.65, making the asperity interference effects a dominant mechanism near threshold. The common feature of all these alloys is that they exhibit nonlinear crack paths because of microstructural barriers and planarity of slip. The work points out the need to include fracture surface information along with the fatigue crack growth rates, especially in coarse-grained and planar-slip alloys.

ACKNOWLEDGMENTS

The work described here was sponsored by the Fracture Control Program, College of Engineering, University of Illinois. Dr. Brian Worth, WPAFB, is thanked for sharing his crack closure data on γ-aluminides, and Dr. A.J. McEvily is thanked for providing closure and roughness data on 9Cr-1Mo steels.

NOMENCLATURE

σ_0	standard deviation of heights of a surface
ν	Poisson's ratio
C	nondimensional constant, $[p_0^s/E^*]^2$ [2 ln $(4E^*/p_0^s)$ − 1]
c_i	initial crack length
COD	crack opening displacement
E^*	plane strain elastic modulus
k	yield stress in shear
N	number of asperities per unit length
p_0^s	shakedown pressure
Q/P	tangential traction coefficient
R_0	asperity tip radius
S_{max}	far-field maximum stress
S_{min}	far-field minimum stress
S_{open}	crack opening stress
S_y	yield stress
z	asperity height

REFERENCES

1. S. Suresh: *Fatigue of Materials*, Cambridge University Press, Cambridge, United Kingdom, 1991.
2. H. Sehitoglu, K. Gall, and A.M. Garcia: *Int. J. Fract.*, 1997, vol. 80 (2–3), pp. 165-92.
3. A. Garcia and H. Sehitoglu: *Metall. Mater. Trans. A*, 1997, vol. 28A, pp. 2263-75.
4. R. Ritchie, W. Yu, A. Blom, and D. Holm: *Fatigue Fract. Eng. Mater. Struct.*, 1987, vol. 10 (5), pp. 343-62.
5. R.D. Carter, E.W. Lee, E.A. Starke, and C.J. Beevers: *Metall. Trans. A*, 1984, vol. 15A, pp. 553-63.
6. C.P. Blankenship and E.A. Starke: *Fatigue Fract. Eng. Mater. Struct.*, 1991, vol. 14, pp. 103-14.
7. D. Krueger, S.D. Antolovich, and R.H. Van Stone: *Metall. Trans. A*, 1987, vol. 18A, pp. 1431-49.
8. G.T. Gray III, J.C. Williams, and A.W. Thompson: *Metall. Trans. A*, 1983, vol. 14A, pp. 421-33.
9. S. Suresh: *Metall. Mater. Trans. A*, 1983, vol. 14A, pp. 2375-85.
10. K. Gall, H. Sehitoglu, and Y. Kadioglu: *Acta Metall.*, 1996, vol. 44 (10), pp. 3955-65.
11. N. Walker and C.J. Beevers: *Fatigue Eng. Mater. Struct.*, 1979, vol. 1, pp. 135-48.
12. J.M. Larsen: Ph.D. Thesis, Carnegie Mellon University, Pittsburgh, PA, 1987.

13. J.E. Allison, R.C. Ku, and M.A. Pompetzki: ASTM STP 982 171-185, ASTM, Philadelphia, PA, 1988.
14. T. Ogawa and K. Tokaji: *Fatigue Fract. Eng. Mater. Struct.*, 1993, vol. 16 (9), pp. 973-82.
15. A. Ohtsuka: *Eng. Fract. Mech.*, 1975, vol. 7, p. 429.
16. K. Minakawa and A.J. McEvily: *Scripta Metall.*, 1981, vol. 15, pp. 633-36.
17. A. Kapoor and K.L. Johnson: *Leeds-Lyon Symp. on Tribology*, 1993, pp. 81-90.
18. K.L. Johnson and H.R. Shercliff: *Int. J. Mech Sci.*, 1992, vol. 34 (5), pp. 375-94.
19. V. Bhargava, C. Rubin, and G.T. Hahn: *ASME, J. Appl. Mech.*, 1983, vol. 52, pp. 66-82.
20. Y. Jiang and H. Sehitoglu: *Wear*, 1996, vol. 191, pp. 35-44.
21. S.J. Balsone, J.M. Larsen, D.C. Maxwell, and W.J. Jones: *Mater. Sci. Eng.*, 1995, vols. A192–A193, pp. 457-64.
22. H. Sehitoglu and W. Sun: *ASME, J. Eng. Mater. Technol.*, 1991, vol. 113, pp. 31-41.
23. J.E. Allison and J.C. Williams: *Titanium Science and Technology*, G. Lujtering, U. Zwicker, and W. Burk, eds., DGM Publishers, Oberusel, 1985, vol. 1, pp. 2243-50.
24. H. Bao and A.J. McEvily: *Metall. Mater. Trans. A*, 1995, vol. 26A, pp. 1725-33.
25. A. McEvily: private communication, University of Connecticut, 1996.
26. B. Cotterell and J. Rice: *Int. J. Fract.*, 1980, vol. 16, pp. 155-169.